Chemical Engineering Journal 166 (2011) 704–709

Contents lists available at ScienceDirect

Chemical Engineering Journal

journal homepage: www.elsevier.com/locate/cej

Simulation of direct reduction reactor by the grain model

S.M.M. Nouri, H. Ale Ebrahim*, E. Jamshidi

Department of Chemical Engineering, Amirkabir University of Technology, Petrochemical Center of Excellency, Tehran 15875-4413, Iran

ARTICLE INFO

Article history:
Received 3 May 2010
Received in revised form
20 September 2010
Accepted 6 November 2010

Keywords:
Simulation
Direct reduction
Moving bed reactor
Grain model

ABSTRACT

In this work, a mathematical model is developed for simulating the behavior of a direct reduction moving bed reactor for the production of sponge iron. The pellet scale model is based on a grain model with product layer resistance. The reactor is modeled through a nonisothermal, steady state, heterogeneous model. Model predictions show good agreement with the data of Foolad Mobarake plant (Isfahan, Iran). Finally, the effects of reducing gas parameters and pellet characteristics on the reduction extent have been investigated.

1. Introduction

The field of noncatalytic gas solid reactions has been and is still a very active research area in chemical engineering. Industrial processes such as direct reduction of metallic oxides [1–3], gasification of coal [4], roasting of mineral sulfide ores [5], adsorption of acidic gases [6] and regeneration of coked catalysts [7] are only some of the applications of these reactions.

The direct reduction process is commercially used for the production of sponge iron by reducing gases from steam and the dry reforming of natural gas. In the moving bed reactor, the reducing gas mixture flows upward and counter-current to the downward flow of solids and reduces the hematite pellets. The overall reaction scheme can be simplified to:

$$Fe_2O_3 + 3H_2 \rightarrow 2Fe + 3H_2O \quad (1)$$

$$Fe_2O_3 + 3CO \rightarrow 2Fe + 3CO_2 \quad (2)$$

In the past three decades, the subject of direct reduction of iron oxides has been studied by presenting some mathematical models.

At pellet scale, the unreacted shrinking core model (neglecting pellet porosity) is an assumption that most of the previous models have used [8–10]. This model provides an overall interpretation of experimental data very well, but experiments also show that the reacted and unreacted zones in a pellet are not separated by a sharp boundary. In fact, metallographic examination of partially reduced iron oxide pellets indicated that the reacted and unreacted zones were separated by a transition section.

Some of the reactor models include only one reacting gas. Most of the models have used pure H_2 [9,11–14], pure CO [15] or a mixture of H_2 and CO as reducing gas [16,17]. Whereas reducing gas at a practical direct reduction reactor is a mixture of H_2, CO, H_2O, CO_2 and CH_4. Recently, the moving bed direct reduction reactor has been modeled by unreacted shrinking core model for two industrial plants [18].

Using constant values for gas and solid physical and chemical properties is another simplifying assumption that most of the previous models have used. For example, most models have applied the constant value for diffusion or some have estimated it as a linear function of temperature.

In this work, the grain model with product layer resistance has been developed to simulate the direct reduction reactor. This model considers intergrain diffusion of the porous hematite pellet as well as the product layer (sponge iron) diffusion around each grain. The kinetics from this model is inserted into the mass and heat balance equations of the moving bed direct reduction reactor. The modeling results have been compared with Foolad-e-Mobarake plant data successfully. Finally, the effect of operating parameters on the reactor performance has been studied by a simulation program.

2. Mathematical model

The mass and energy balance equations with boundary conditions are presented here. Some of the general necessary

* Corresponding author. Tel.: +98 2166405847; fax: +98 2166405847.
E-mail addresses: mehdi.nori@aut.ac.ir (S.M.M. Nouri), alebrm@aut.ac.ir (H. Ale Ebrahim).

1385-8947/$ – see front matter © 2010 Elsevier B.V. All rights reserved.
doi:10.1016/j.cej.2010.11.025

Nomenclature

a	dimensionless gas concentration, C_A/C_{Ab}
A_p	outer surface area of the pellet
b	stochiometric coefficient
C_{Ab}	reactant gas concentration in the bulk
C_{pg}, C_{ps}	heat capacity for gas and solid phases
D_{AK}	Knudsen diffusivity of gas "A"
D_{AM}	molecular diffusivity
D_e	effective diffusivity of gas "A" in the pellet
D_p	diffusivity in the product layer
E	porosity of bed
F_g	shape factor of the grains
F_p	shape factor of the pellet
G_{mg}, G_{ms}	gas and solid molar flows
h	heat transfer coefficient
k	reaction rate constant
k_g	gas film layer mass transfer coefficient
l	reactor length from top
L	total reactor length
M_w	molecular weight
n_p	number of pellets per unit volume of the bed
N_{Nu}, N_{Re}	Nusselt and Reynolds numbers, respectively
N_{Sc}, N_{Sh}	Schmidt and Sherwood numbers, respectively
Q	gas flow-rate
R	reaction rate per pellet
R_g	gas constant
r	pellet radius
r_{gc}	unreacted core radius in each grain
r_{g0}	initial grain radius
r^*	dimensionless unreacted radius in the grain, r_{gc}/r_{g0}
T_g, T_s	gas and solid phase temperatures
t	time
u_g, u_s	gas and solid velocity
X	solid conversion
y	dimensionless position in the pellet

Greek letters

ΔH	heat of reaction
ε	pellet porosity
$\theta = kC_{Ab}M_Bt/\rho_Br_{g0}$	dimensionless time for the grain model
$\sigma = r\sqrt{F_gk(1-\varepsilon)/D_er_{g0}}$	reaction modulus for the pellet
$\sigma_g = \sqrt{kr_{g0}/2D_pF_g}$	reaction modulus for the grains

assumptions for derivation of these equations are as follows [19,20]:

(1) steady state operation
(2) plug flow for both gas and solid stream in the reactor
(3) the pellets diameter remains constant during the reaction
(4) the pellet composed of fine spherical grains
(5) catalytic effects may be neglected
(6) ideal gas mixture
(7) irreversible and first order reactions

2.1. Pellet modeling

In this work, a grain model with product layer resistance is used as a new approach for the modeling of direct reduction in a moving bed reactor of hematite. This model is based on the following assumptions:

(1) pseudo-steady state approximation
(2) the pellet is isothermal
(3) diffusion resistance through the product layer of each grain is taken into account
(4) spherical pellet geometry
(5) equimolar counter diffusion system

The general form of the dimensionless equations which describe the pellet behavior is as follows [21]:

$$\frac{1}{y^2}\frac{\partial}{\partial y}\left(y^2\frac{\partial a}{\partial y}\right) = \frac{\sigma^2 r^{*2} a}{1+6\sigma_g^2(r^*-r^{*2})} \tag{3}$$

$$\frac{\partial r^*}{\partial \theta_{pl}} = -\frac{a}{1+6\sigma_g^2(r^*-r^{*2})} \tag{4}$$

There is no analytical solution for the above coupled partial differential equations. Hence, we use Sohn's assumption to reach an approximate solution [21].

When σ approaches zero, r^* approaches unity everywhere and the integration of Eq. (3) gives:

$$\theta_{pl_{\sigma=0}} = g_{Fg}(X) + \sigma_g^2 \cdot P_{Fp}(X) \tag{5}$$

For spherical grains and pellet we have:

$$g_3(X) = 1-(1-X)^{1/3} \tag{6}$$

$$P_3(X) = 1-3(1-X)^{2/3}+2(1-X) \tag{7}$$

And when σ approaches infinity, the intrapellet diffusion becomes the only rate controlling step and the gaseous reactant concentration at the interface between unreacted and reacted zone in the grains drops to zero. Therefore, we have:

$$\theta_{pl_{\sigma\to\infty}} = \sigma^2 \cdot p_3(X) \tag{8}$$

By combination of Eqs. (5) and (8), and external mass transfer resistance, the approximate conversion-time relation can be presented as follows [20]:

$$\frac{bkC_{Ab}t}{\rho_Br_{g0}} = 1-(1-X)^{1/3}+\left(\frac{kr_{g0}}{6D_P}+\frac{kr_0^2(1-\varepsilon)}{6D_er_{g0}}\right)[1-3(1-X)^{2/3}+2(1-X)]+\frac{2}{Sh}\times\frac{kr_0^2(1-\varepsilon)}{6D_er_{g0}}X \tag{9}$$

By extracting dX/dt from Eq. (9), the reaction rate for each gaseous reactant is expressed as follows:

$$R\ \left(\frac{\text{mole}}{\text{m}^3\ \text{s}}\right) = \frac{-bkC_{Ab}(1-\varepsilon)(1-E)/r_{g0}}{1/3(1-X)^{2/3}+(kr_{g0}/6D_p+kr_0^2(1-\varepsilon)/6D_er_{g0})(2/(1-X)^{1/3}-2)+kr_0^2(1-\varepsilon)/3D_{AM}r_{g0}(2+0.39Re^{1/2}Sc^{1/3})} \tag{10}$$

2.2. Reactor modeling

The mass balance equations for gaseous reactants based on Eq. (10) for the reaction rate, can be stated as follows [18]:

$$u_g\frac{dC_{H_2}}{dl}+n_pR_{H_2}=0 \tag{11}$$

$$u_g\frac{dC_{CO}}{dl}+n_pR_{CO}=0 \tag{12}$$

Mass balance on the reactant solid may be written as follows:

$$u_s\frac{dC_{Fe_2O_3}}{dl}+\frac{n_p}{b}(R_{H_2}+R_{CO})=0 \tag{13}$$

Energy balance for gas and solid phases can be written as follows [18]:

$$G_{mg}C_{pg}\frac{dT_g}{dl} + n_p A_p h(T_g - T_s) = 0 \quad (14)$$

$$G_{ms}C_{ps}(C_s, T_s)\frac{dT_s}{dl} + n_p[A_p h(T_s - T_g) + \Delta H_{H_2}(T_s)R_{H_2} + \Delta H_{CO}(T_s)R_{CO}] = 0 \quad (15)$$

Boundary conditions for the above equations are as follows:

$$C_{H_2}(l = L) = C^0_{H_2}, \quad C_{CO}(l = L) = C^0_{CO} \quad (16)$$

$$C_{Fe_2O_3}(l = 0) = C^0_{Fe_2O_3} \quad (17)$$

$$T_g(l = L) = T^{in}_g, \quad T_s(l = 0) = T^{in}_s \quad (18)$$

The above mathematical modeling of the moving bed direct reduction reactor leads to a set of nonlinear ordinary differential equations with a set of split boundary conditions. These differential equations are solved using a Runge–Kutta method called Shooting method. Shooting method transforms the boundary value problem into an initial value problem and then the resulting equations are solved by the Runge–Kutta method.

2.3. Parameter calculation

2.3.1. Kinetic constants

The kinetic equations for hematite reduction by hydrogen and carbon monoxide are used from Ref. [18] as follows:

$$k_{H_2} = 0.225\ \exp(-14700/82.06T)\ \ \text{cm/s} \quad (19)$$

$$k_{CO} = 0.650\ \exp(-28100/82.06T)\ \ \text{cm/s} \quad (20)$$

2.3.2. Heat and mass transfer coefficients

For the pellets in a moving bed reactor, the following empirical equation was stated for the heat transfer coefficient between gas and particles [22]:

$$\text{Nu} = 2 + 0.39Re_P^{1/2} \cdot Pr^{1/3} \quad (21)$$

The mass transfer coefficient between gas and pellets in a moving bed reactor can be obtained using the analogy between heat and mass transfer:

$$\text{Sh}_j = 2 + 0.39Re_P^{1/2} \cdot \text{Sc}_j^{1/3} \quad (22)$$

2.3.3. Diffusion coefficients

The mass transport rate through the porous solid is governed by two phenomena:

(a) Molecular diffusion, which is a property of a gas mixture. When the pore diameter is large compared with the mean free path of gas molecules, molecular diffusion is predominant and may be estimated using the Chapman–Enskog relation [23]:

$$D_{ij} = \frac{4.52 \times 10^{-6}T^{1.75}}{P[2(M_i^{-1} + M_j^{-1})]^{0.5}[(\sum V_i)^{\frac{1}{3}} + (\sum V_j)^{\frac{1}{3}}]^2} \quad (23)$$

(b) Knudsen diffusion, which depends on the molecular velocity and pore size. This diffusivity is predominant in the micropores. The Knudsen diffusivity is given by [24]:

$$D_{AK} = \frac{4}{3}\left(\frac{8R_gT}{\pi \cdot M_A}\right)^{\frac{1}{2}} \cdot \frac{3\pi r_{g0}}{4(\pi + 8)(1 - \varepsilon)} \quad (24)$$

The overall diffusivity obtained from the two above phenomena is given by [24]:

$$\frac{1}{D_e} = \frac{1}{\varepsilon^2}\left(\frac{1}{D_{AM}} + \frac{1}{D_{AK}}\right) \quad (25)$$

Table 1
Operating conditions of Foolad Mobarake plant.

Reactor length	9.1 m	
Reactor diameter	5.5 m	
Bed porosity	0.5624	
Bed density	2 g/cm^3	
Solid properties		
Sponge iron flow rate	110 ton/h	
Reduced iron density	3.2 g/cm^3	
Iron ore density	4.7 g/cm^3	
Gas properties		
Outlet pressure	1.35 bar	
Flow rate	177,180 Nm^3/h	
Intel temperature	1174°	
Outlet temperature	791°	
Gas composition	Inlet gas	Outlet gas
Hydrogen	53.47	32.24
Carbon monoxide	34.25	21.6
Water (vapor)	5.83	25.05
Carbon dioxide	2.6	15.46
Nitrogen and methane	3.65	3.65
Conversion		94.8

Moreover, the diffusions through the product layer (D_p values) are used from Ref. [18] as follows:

$$D_{p,H_2} = 1.467 \times 10^{-6}T^{1.75}\ \ \text{cm}^2/\text{s} \quad (26)$$

$$D_{p,CO} = 3.828 \times 10^{-7}T^{1.75}\ \ \text{cm}^2/\text{s} \quad (27)$$

3. Results and discussion

In this section, a comparison between the predictions of the mathematical model and the plant data is performed. The model presented in the previous section is validated using experimental data from a MIDREX plant (Foolad Mobarake, Isfehan, Iran). The operating conditions of the plant reactor are shown in Table 1.

Results of the simulation model are in good agreement with the plant data. A comparison between them is shown in Table 2. The inlet gas composition used in the model was identical to that of the plant, i.e. those inlet values listed in Table 1.

Fig. 1 shows the temperature profile along the reactor. It can be seen that the temperature profile perfectly satisfies the boundary temperature extracted from the plant data. The gas temperature decreases from bottom (inlet) along the reactor, owing to heat transfer with the solid and the endothermic reactions between iron oxides and reactant gases.

In all of figures of this section, a length of 0 cm corresponds to the outlet for the gas or inlet for the solid (top of the reactor) and length of 900 cm corresponds to the inlet for the gas or outlet for the solid (bottom of the reactor). However, the solid moves counter-currently from top to the bottom of the reactor. These situations were also described by boundary conditions (16)–(18).

Fig. 2 shows the gas composition variation along the reactor. It can be seen that the absolute value of the slope of composition profile for each gas (except inert gases) is quite bigger in the upper part (0 cm) of the reactor. It shows that the total reaction

Table 2
Comparison between model results and plant data.

	Model results	Plant data
Outlet gas composition		
Hydrogen	32.92	32.24
Carbon monoxide	23.32	21.6
Water vapor	26.38	25.05
Carbon dioxide	13.73	15.46
Nitrogen and methane	3.65	3.65
Solid conversion	93.9	94.8

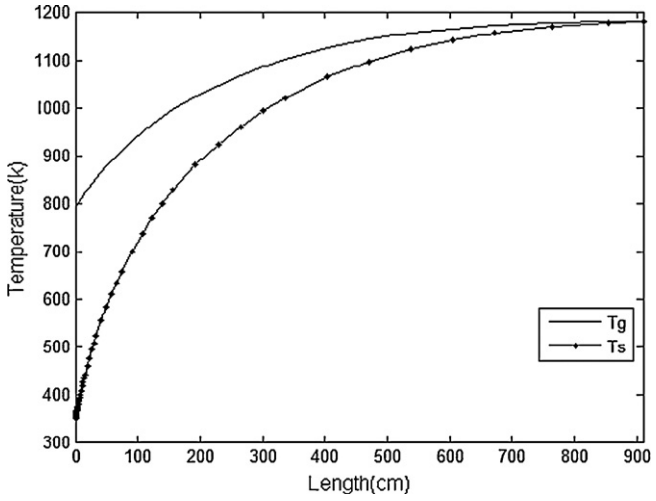

Fig. 1. Gas and solid temperature profiles along the reactor.

rate decreases along the reactor. As a result, the diffusion role (iron thickness around the grains) on controlling the total reaction rate increases from top to bottom of the reactor.

3.1. Effect of gas flow rate

Fig. 3 shows the effect of variation of the reducing gas flow rate on the conversion of iron ore. When the gaseous flow rate is increased, a higher solid conversion is obtained and more gaseous reactants are consumed. This is not caused by the decrease of external mass transfer resistances from gas to solid as the gas velocity is increased. Calculations show that even at the lowest flow rate the Sherwood number is high enough to make the mass transfer resistance negligible. Therefore, the reason is that as the flow rate increases, the concentration of reducing gases at the upper part of the reactor increases.

This matter is verified by comparing the denominator terms of Eq. (10). The first, second and third terms are proportional to reaction resistance, product layer and solid reactant diffusion resistances, and external mass transfer resistance, respectively. For example, these terms are 0.4, 8.8, and 0.03, respectively for hydrogen and at 25% solid conversion. At 75% conversion, these terms become 0.76, 25.7, and 0.02 which show increasing resistance for the product layer (sponge iron) diffusion. Consequently, mass transfer resistance is negligible in all situations.

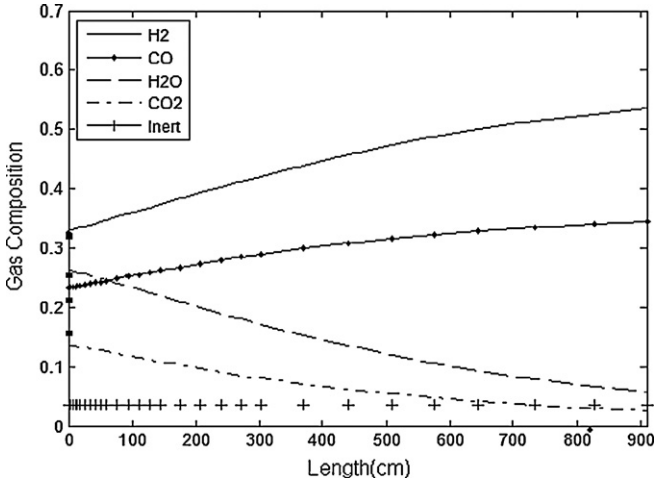

Fig. 2. Gaseous composition profiles along the reactor (points below H_2, H_2O, CO and above CO_2 composition line show outlet gas composition of plant).

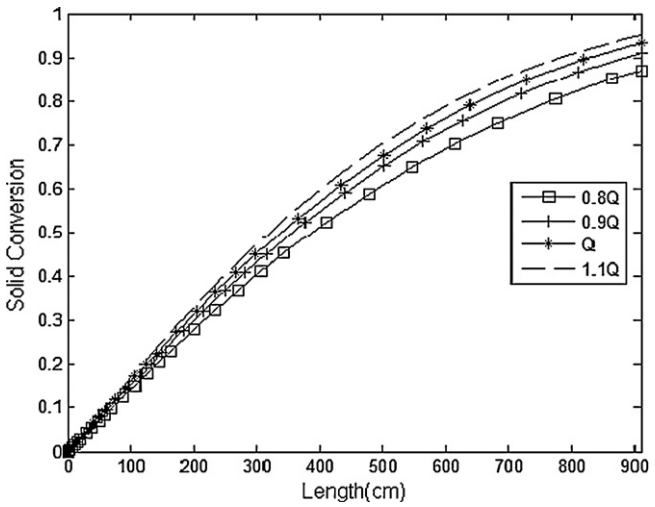

Fig. 3. Effect of gas flow rate on the conversion of iron ore.

3.2. Effect of feed gas composition

Fig. 4 shows the effect of the H_2/CO ratio on the solid conversion. The solid conversion is increased by increase of carbon monoxide concentration (or decreasing the above ratio) in the feed gas. Since the rate constant for carbon monoxide is greater than of hydrogen [choosing Eqs. (19) and (20) in this work] at the same temperature. But, this ratio is highly restricted by the reformer condition and possibility of coke deposition on the sponge iron, and therefore, the H_2/CO ratio is usually more than one.

3.3. Effect of feed gas potential

Fig. 5 shows the effect of feed gas potential on solid conversion. The $(H_2 + CO)/(H_2O + CO_2)$ ratio usually changes within 5–49. This characteristic is changing with the reformer operating conditions and generally remains constant along steady state operations [25]. It can be seen that with increase in the gas potential, solid conversion increases due to the entrance of more reducing gas into the reactor. But increasing the potential ratio more than 20 has no considerable effect on the conversion. Because the operating conditions examined the pellets were nearly fully reduced in all cases.

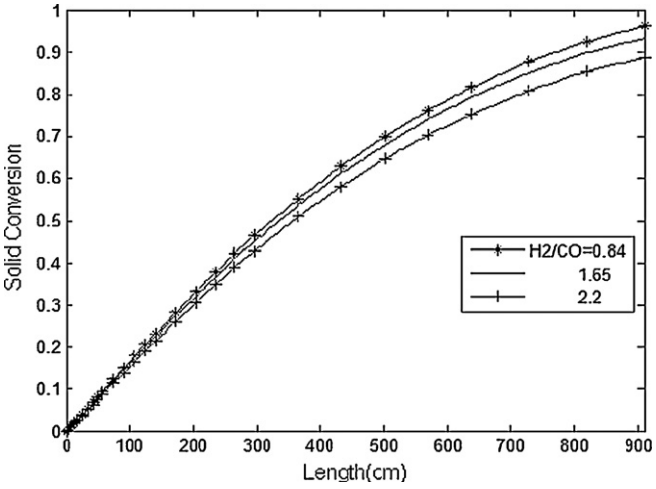

Fig. 4. Effect of feed gas composition on the solid conversion.

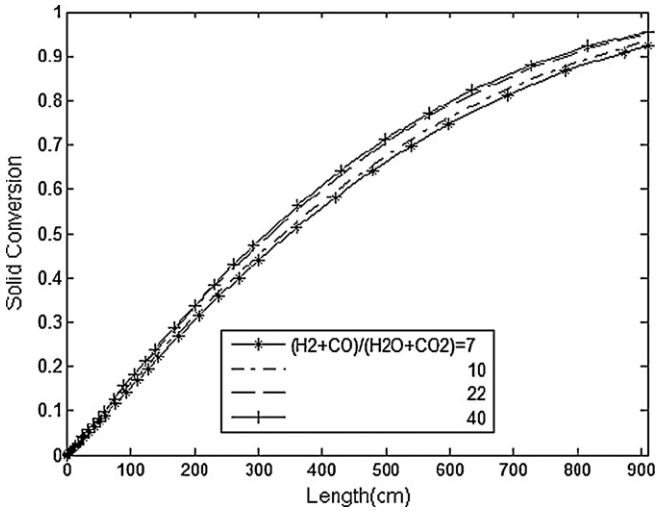

Fig. 5. Effect of gas potential on the solid conversion.

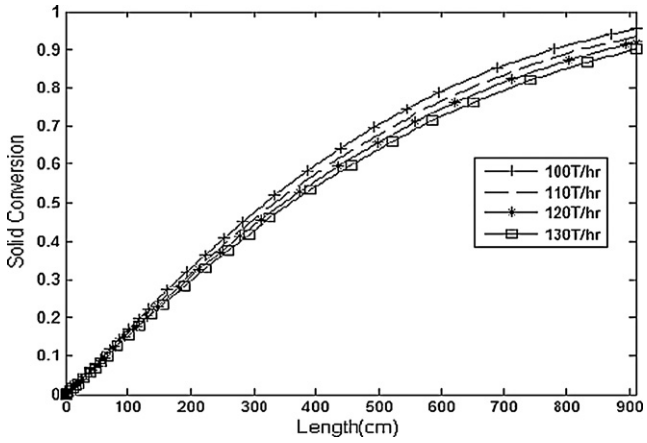

Fig. 6. Effect of solid flow rate on the solid conversion.

3.4. Effect of solid flow rate

Fig. 6 shows the effect of different solid flow rates on the conversion. As the solid flow rate is increased, the conversion of outlet pellets is reduced. When the solid flow rate is increased, the average residence time of iron ore pellets in the reactor is decreased and the solid particles have less time to react with the gaseous reactants. However, if the gas flow rate is kept constant, the reducing gas will contact more fresh solid and its reduction potential is decreased.

3.5. Effect of reactor length

The effect of increasing the reactor length is very similar to the effect of decreasing the solid flow. Increase of the bed length increases the solid conversion of iron ore particles, because the mean residence time of solid particles is increased. Table 3 shows the influence of increasing the reactor length.

Table 3
Variation of solid conversion with the reactor length.

Reactor length (cm)	Solid conversion
750	0.87
850	0.91
910	0.93
950	0.94

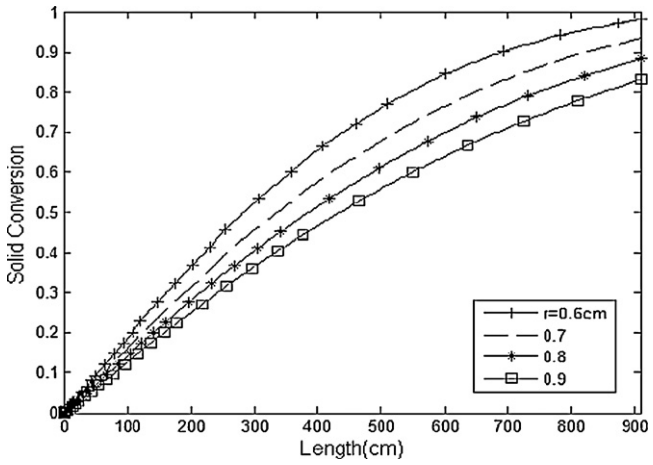

Fig. 7. Effect of pellet size on the solid conversion.

3.6. Effect of pellet size

The effect of pellet size on the conversion of solid is illustrated in Fig. 7. It can be seen that when the size of the pellets is increased, a considerable decrease in solid conversion will result because pellets with a larger diameter need more time to reduce completely.

3.7. Comparison of porous and nonporous models

Comparison between porous (grain model) and nonporous (unreacted shrinking core model) models for the direct reduction is important. The nonporous models are usually the old gas–solid reaction models and have been used for some reactions because of their mathematical simplicity (product layer diffusion and reaction in series) [26]. However, the initial solid reactant pellet is seldom completely nonporous, especially at industrial scale where higher reactivity is required. Therefore, using the porous models can express the behavior of the system (parallel solid reactant diffusion with reaction and product layer diffusion) more accurately. The solid conversion profiles for the direct reduction system are presented in Fig. 8, for nonporous and porous models. As this figure shows, the grain model (this work) predicts the final metallization point of Foolad Mobarake very well. While, unreacted shrinking core model underestimates the plant metallization point considerably, due to assumption of nonporous initial hematite pellet.

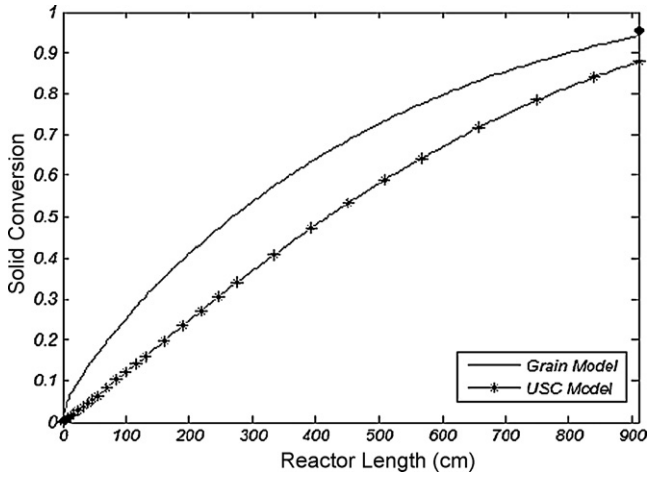

Fig. 8. Solid conversion for Folad Mobarake plant data using unreacted shrinking core (USC) model and grain model, the point (•) at the bottom of reactor is the conversion of solid from the plant data.

4. Conclusion

In this work, moving bed reactor of direct iron ore reduction was simulated by a one dimensional heterogeneous model. Grain model with product layer resistance was applied to predict the reaction–diffusion phenomena in the pellet size. The results of the model were in a good agreement with the Foolad Mobarake industrial plant data.

The effects of gas, pellet and reactor parameters were investigated by a simulation model. It was found that the solid conversion will increase by increasing the gas flow rate or its reducing potential. Moreover, reduction of small iron ore pellets requires lower residence times to reach complete conversion compared to pellets of larger diameter. The effect of H_2/CO ratio was also investigated and the results show that by increasing the H_2/CO ratio, solid conversion decreased. Finally, the grain model prediction was compared to shrinking unreacted core model and plant data.

References

[1] J. Szekely, C.I. Lin, H.Y. Sohn, A structural model for gas–solid reactions with a moving boundary. V. An experimental study of the reduction of porous nickel oxide pellets with hydrogen, Chem. Eng. Sci. 28 (1973) 1975–1989.
[2] K.L. Breg, S.E. Olsen, Kinetics of manganese ore reduction by carbon monoxide, Metall. Mater. Trans. B 31 (2000) 477–490.
[3] H. Ale Ebrahim, E. Jamshidi, Kinetic study and mathematical modeling of the reduction of ZnO–PbO mixtures by methane, Ind. Eng. Chem. Res. 44 (2005) 495–504.
[4] E.A. Delikouras, D.D. Perlmuter, Combined effects of mass transfer and inaccessible porosity in gasification reactions, AIChE J. 39 (1993) 829–835.
[5] S. Kimura, Oxidation kinetics of polycrystalline zinc sulfide grains, AIChE J. 35 (1989) 339–342.
[6] H. Ale Ebrahim, Application of random pore model to SO_2 capture by lime, Ind. Eng. Chem. Res. 49 (2010) 117–122.
[7] D. Bai, J.X. Zhu, Y. Jin, Z. Yu, Simulation of FCC catalyst regeneration in a riser regenerator, Chem. Eng. J. 71 (1998) 97–109.
[8] J. Szekely, Y. El-Tawil, The reduction of hematite pellets with carbon monoxide-hydrogen mixtures, Metall. Trans. B 7B (1976) 490–492.
[9] E.T. Turkdogan, J.V. Vinters, Gaseous reduction of iron oxides: part I. Reduction of hematite in hydrogen, Metall. Trans. 2 (1971) 3175–3188.
[10] N. Towhidi, J. Szekely, Reduction kinetics of commercial low-silica hematite pellets with CO–H_2 mixture over temperature range 600–1234 °C, Ironmaking Steelmaking 6 (1981) 237–249.
[11] W.M. McKewan, Influence movement during high pressure reaction of hematite by hydrogen, J. Metals 16 (1964) 781–802.
[12] W.M. McKewan, Reduction kinetics of hematite in hydrogen–water vapor–nitrogen mixtures, Trans. Metal. Soc. AIME 224 (1962) 2–5.
[13] R.H. Spitzer, F.S. Manning, Mixed control reaction kinetics in the gaseous reduction of hematite, Trans. Metal. Soc. AIME 23 (1963) 6726–6742.
[14] T. Usui, M. Ohmi, E. Yamamura, Analysis of rate of hydrogen reduction of porous wustite pellets basing on zone reaction models, ISIJ Int. 30 (1990) 347–355.
[15] R.H. Tien, E.T. Turkdogan, Gaseous reduction of iron oxides: part IV. Mathematical analysis of partial internal reduction–diffusion control, Metall. Trans. 3 (1972) 2039–2048.
[16] E.K.T. Kam, R. Hughes, A model for the direct reduction of iron ore by mixtures of hydrogen and carbon monoxide in a moving bed, Trans. IChmE 59 (1981) 196–206.
[17] E.D. Negri, O.M. Alfano, M.G. Chiovetta, Direct reduction of hematite in a moving bed reactor. Analysis of the water gas shift reaction effects on the reactor behavior, Ind. Eng. Chem. Res. 30 (1991) 474–482.
[18] D.R. Parisi, M.A. Laborde, Modeling of counter current moving bed gas–solid reactor used in direct reduction of iron ore, Chem. Eng. J. 104 (2004) 35–43.
[19] O. Levenspiel, Chemical Reaction Engineering, John Wiley, New York, 2003.
[20] J. Szekely, J.W. Evans, H.Y. Sohn, Gas–Solid Reactions, Academic Press, New York, 1976.
[21] H.Y. Sohn, J. Szekely, The effect of intragrain diffusion on the reaction between a porous solid and a gas, Chem. Eng. Sci. 29 (1974) 630–634.
[22] T. Akiyama, R. Takahashi, J. Yagi, Measurements of heat transfer coefficients between gas and particles for a single sphere and for moving beds, ISIJ Int. 33 (1993) 703–710.
[23] R.B. Bird, W.E. Stewart, E.N. Lightfoot, Transport Phenomena, John Wiley, New York, 2002.
[24] M.J. Proctor, R.J. Hawkins, J.D. Smith, Reduction of iron ore pellets in CO–CO_2–H_2–H_2O mixtures, Ironmaking Steelmaking 19 (1994) 194–200.
[25] Y. Takenaka, Y. Kimura, K. Narita, D. Kaneko, Mathematical model of direct reduction shaft furnace and its application to actual operations of a model plant, Comput. Chem. Eng. 10 (1986) 67–75.
[26] P.A. Ramachandran, L.K. Doraiswamy, Modeling of noncatalytic gas–solid reactions, AIChE J. 28 (1982) 881–900.